Progress In Electromagnetics Research C, Vol. 135, 145–156, 2023

Finite Element Analysis on Doubly Salient Singly Excited Machine for Electrified Transportation Systems

Sundaramoorthy Prabhu[1, *], Vijayakumar Arun[1], Balaji Mahadevan[3], Peruthambi Venkatesh[1], Puluru V. Aravindha Reddy[2], Sane Siva Mohan[2], Sareddy Raju Kumar Reddy[2], and Somu Santhosh Kumar Reddy[2]

Abstract—Doubly Salient Singly Excited Machine (DSSEM) inbuilt with the features as high torque density, high speed density, compactness, low maintenance, but the machine reduces its application due to its demerits as torque ripple. This study enhances the performance of switched reluctance motor (SRM) in the track of electromagnetic and mechanical characteristics. A 290 Volts, 10 Amps, 3000 rpm, 4 N-m SRM undergoes finite element (FE) characterization in the view of parameters like torque ripple. In the regard of torque characterization, the ripple torque is estimated under rated condition. FE analysis gives accurate results by 2D analysis. Torque ripple is the main concern in electrical machines, because these two are responsible for producing harmonics, vibration, and noise. So, a novel machine is designed to reduce the torque ripple content. The losses are considered as heat generation as a source of temperature rise in a motor, and the heat distribution is analyzed. The experimental setup is arranged to evaluate the simulation results with the current profile of FE analysis and prototype for verification.

1. INTRODUCTION

The reduction of torque ripple of SRM is one of the hot issues in the field of electrical machine design. The optimal combinations of geometric parameters are determined to reduce torque ripple of SRM. The geometric parameters are divided into two categories based on their impact on the torque ripples of SRM, and a range analysis is conducted. Undesirable torque ripples are present in the SRM due to the spatial Harmonics. By using an optimized current trajectory, torque ripple is reduced. The torque ripple is analysed based on the actual torque map. Torque map is also used for torque reconstruction [1, 2]. For torque density enhancement and torque ripple reduction in a permanent magnet (PM) motor, a novel rotor is designed. Both the proposed and existing PM machines are designed and optimized with the same 8-slot/6-pole stator with nonoverlapping windings as well as the same rotor diameter. The multi-objective optimization design of SRM is a big problem due to its computational cost of Finite Element Analysis (FEA). To get a better performance by making smaller ripple torque and decreased power loss, a method is proposed known as Kriging model, which decreases the computation and can also be applied to higher dimension's machine [3, 4]. The torque ripple in SRM is enhanced by adopting a multi-layer structure in the stator, which helps to reduce the radial magnetic field. The *d-q* parameters and phase flux linkage harmonics are studied to relate between the *d-q* parameters and torque ripple. The winding placement in a 6-pole 12-slot SRM is considered in the study, for ripple torque optimization, to distribute the electromagnetic field equally, and to reduce the vibrations [5, 6]. The electromagnetic exciting force of an Integrated Starter and Generator is reduced which results in Noise and Vibrations

Received 1 May 2023, Accepted 11 July 2023, Scheduled 29 July 2023

* Corresponding author: Sundaramoorthy Prabhu (prabhuphd1987@gmail.com).

[1] Department of Electrical and Electronics Engineering, Mohan Babu University, Tirupati, India. [2] Department of Electrical and Electronics Engineering, Sree Vidyanikethan Engineering College, Tirupati, India. [3] Department of Electrical and Electronics Engineering, Sri Sivasubramaniya Nadar College of Engineering, Chennai, India.

caused from the tangential, radial force and torque ripples of the ISG. This can be done by either improving the stiffness of stator or reducing the excitation electromagnetic force. The main problem with SRM is vibration and noise. Maximum torque per ampere (MTPA) control technique improves the efficiency and torque production. The frequency of vibrations of SRM is understood before conducting a comprehensive analysis of voltage inverter's influence of SRM [7, 8]. The parameter causing the vibration in SRM under load conditions is the radial electromagnetic (EM) force. An advanced inverse cosine function (AICF) is used to reduce the torque ripple of SRM. The non-sinusoidal wave is converted as sinusoidal wave when being disturbed. Fractional Slot Concentrated Winding (FSCW) switched reluctance motor is the most promising machine in the Electrical Vehicle machine design. When SRM drives use Sinusoidal Pulse Width Modulation, high-frequency side bands are inevitable result. This can be reduced by reducing carrier frequency, decreasing switching frequency, reducing pulse width, optimizing modulation index, and digital filtering [9, 10].

2. TORQUE RIPPLE ESTIMATION

Torque ripple is a phenomenon that occurs in every machine, which increases the instability, wear and tear of the machine, and so the life span of the machine [11]. Machine performance, which provides valuable insights into various aspects such as cogging torque, vibrations, acoustic noise, and efficiency mapping, plays a crucial role in assessing and characterizing the behavior and performance of the machine [12].

$$T_r = (3/2) * (K_q * I_q * \lambda_m) / (\Pi * Ld * \phi_d) \tag{1}$$

where T_r = torque ripple, K_q = quadrature-axis inductance factor, I_q = quadrature-axis current, I_d = direct-axis inductance, and ϕ_d = direct-Axis flux

$$T_r = \left(0.5 * nm * I_{ph}^2 \left(L_d - L_q\right)\right) / (\Pi * (L_d + L_q)) \tag{2}$$

where n = no. of phases, m = no. of rotor poles, I_{ph} = phase current, and L_d = direct-axis inductance. Torque ripple in an SRM is affected by the flux distribution throughout the rotor. The relation is as shown below.

$$\Delta T = (1/2) * (B_{\max} * At)^2 * \left(\delta_g^3/3\right) \tag{3}$$

Here At = area of rotor pole face in sq $\cdot$ m.

3. 2D FEA ANALYSIS OF DIFFERENT DESIGNS OF SRM

3.1. Conventional SRM

This section explicitly details the processing of the proposed model. Specific problems regarding torque ripple analysis and approaches to reducing torque ripples are examined, and the proposed scheme is refined. This section verifies the accuracy and reliability of the proposed scheme through simulation and comparison of the performance with several well-known schemes [13].

The conventional type rotor is as shown in Fig. 1, which is compared with the novel machine design, to decrease the torque ripple values of the machine and to increase the maximum torque. Different designs of SRM are introduced for propulsion systems and are tested with FEA software, where flux function is obtained along with temperature, magnetic intensity, and magnetic flux density functions. The torque vs rotor angle position curve of a Switched Reluctance Motor (SRM) shows the variation of torque generated by the motor with respect to the angle of the rotor. The torque generated by an SRM is typically nonlinear and varies based on the position of the rotor. This is due to the magnetic flux path changing as the rotor moves, which causes variations in the reluctance torque. The torque generated by an SRM is also affected by various operating factors, such as the current and voltage supplied to the motor, the number of stator and rotor poles, and the shape of the rotor and stator poles. Additionally, the SRM typically generates cogging torque due to the interaction between the rotor and stator poles, but this can be minimized through design modifications. The torque vs rotor angle position curve of an SRM can be used to model the motor's behavior and optimize its performance for specific applications.

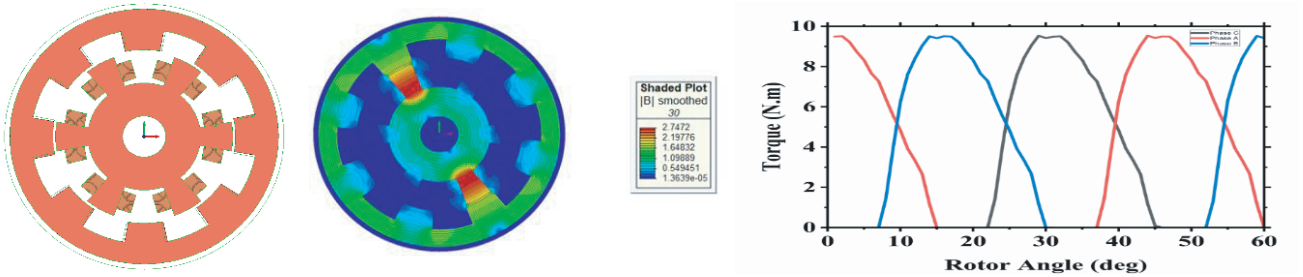

(a) (b) (c)

Figure 1. Switched reluctance hub motor. (a) FEA model. (b) Flux path. and flux density distribution. (c) Torque characteristics.

3.2. Flux Barrier Embedded No Material

Making the Flux Barriers increases the reluctance of the machine, i.e., increase in opposition to the flux passage. Make the machine to follow reluctance principal norms. Flux Function of no-material SRM is shown in Fig. 2. The torque value is increased to 8.65 N-m, and torque ripple is increased to 0.66 N-m [14].

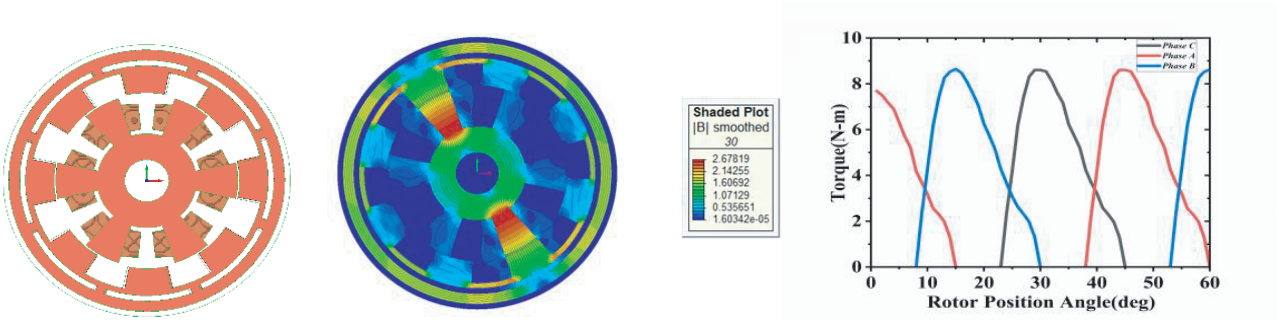

(a) (b) (c)

Figure 2. Embedded no-material into SRM. (a) FEA model. (b) Flux density and flux pattern of SRM. (c) Torque characteristics of SRM.

3.3. Flux Barrier Embedded Magnetic Material

Non-magnetic material is inserted into the slots of flux barriers as shown in Fig. 3. The flux function is similar to the no-material embedded into SRM rotor [15]. The torque value is increased to 7.72 N-m, and torque ripple is increased to 0.84 N-m.

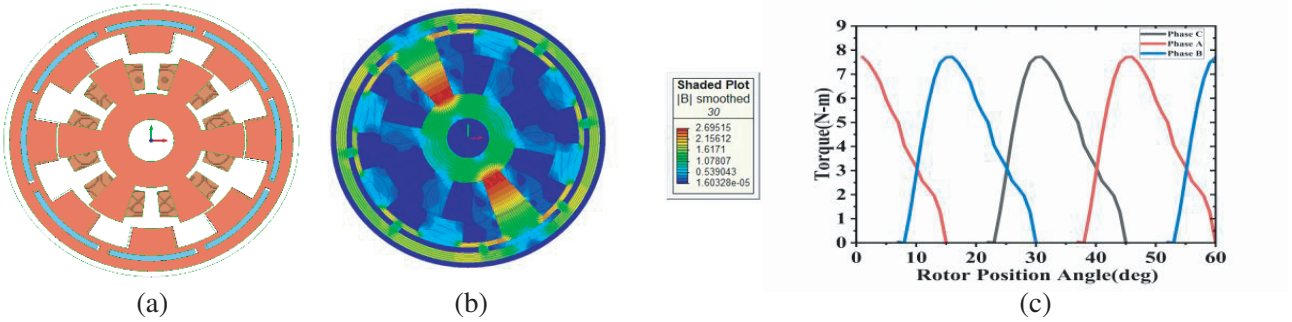

(a) (b) (c)

Figure 3. Embedded magnetic material into SRM. (a) FEA model. (b) Flux density and flux pattern of SRM. (c) Torque characteristics of SRM.

3.4. Increased Flux Barrier Embedded No-Material and Slight down Cut Rotor

The flux barriers of the SRM are increased, as illustrated in Fig. 4, with a slight cut down for the rotor teeth embedded with no-magnetic material. This leads to an increase in the flux density at the edges of the rotor teeth [16]. Consequently, the torque value rises to 10.77 N-m, and the ripple also increases to 1.38 N-m.

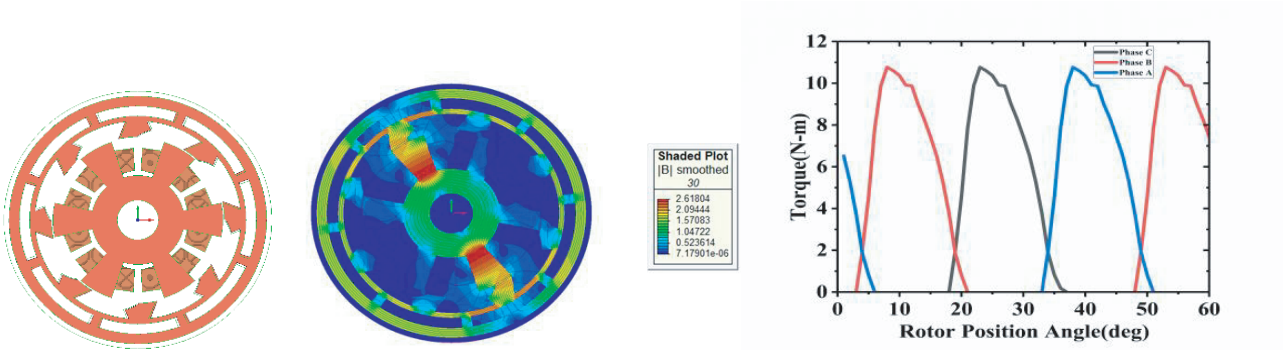

Figure 4. Increased flux barrier embedded no material into SRM. (a) FEA model. (b) Flux density and flux pattern of SRM. (c) Torque characteristics of SRM.

3.5. Decreased Flux Barrier Embedded No Material and Slight Down Cut Rotor

The flux barriers of the SRM are reduced as depicted in Fig. 5, achieved by implementing a down cut and embedding a no material [17]. Consequently, the torque value increases to 13.16 N-m, and ripple is decreased to 0.98 N-m.

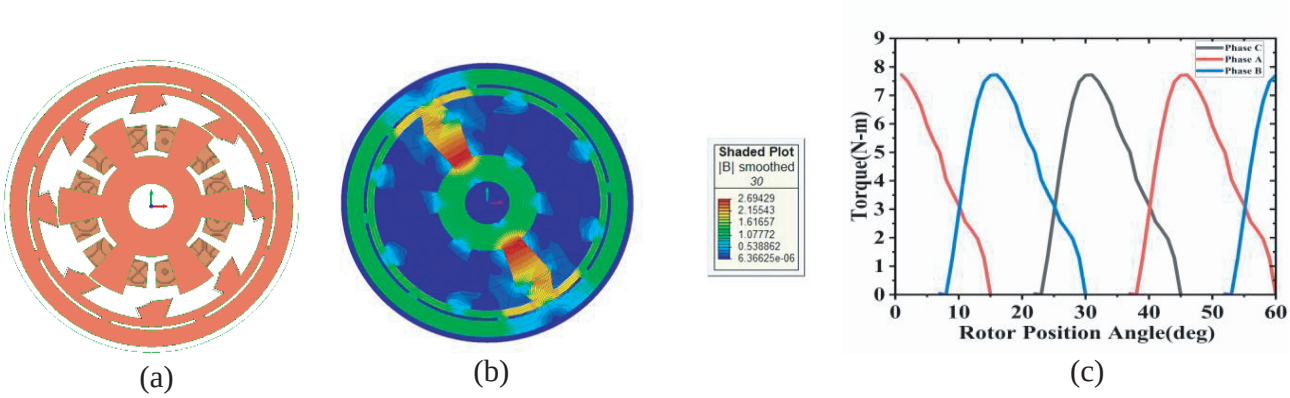

Figure 5. Decreased flux barrier embedded no material into SRM. (a) FEA model. (b) Flux density and flux pattern of SRM. (c) Torque characteristics of SRM.

3.6. Decreased Flux Barrier Embedded Non-Magnetic Material and Slight Down Cut Rotor

Then for the decreased flux barrier a non-magnetic material is embedded into the rotor, and flux function for SRM, flux passage and torque angle curve of embedded non-magnetic material into decreased flux barriers as shown in Fig. 6 [18]. The torque value is increased to 13.55 N-m, and ripple is decreased to 0.94 N-m.

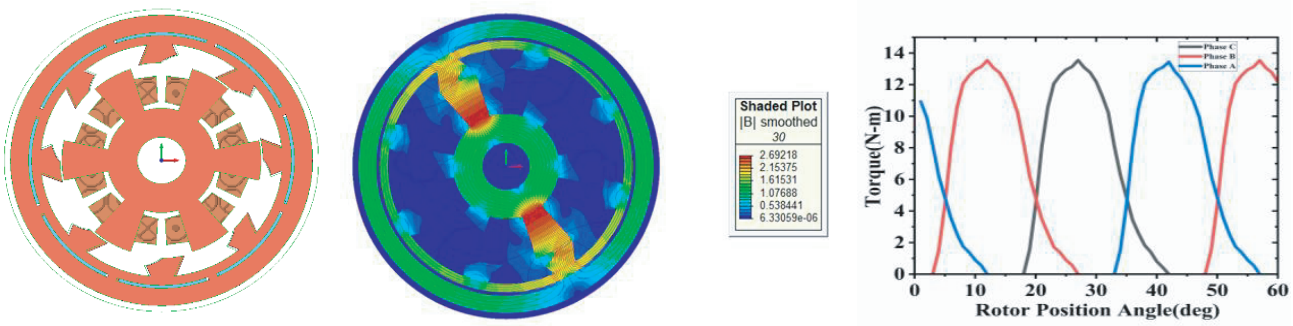

(a) (b) (c)

Figure 6. Decreased flux barrier embedded non-magnetic material into SRM. (a) FEA model. (b) Flux density and flux pattern of SRM. (c) Torque characteristics of SRM.

3.7. Asymmetric Rotor

The decrease in flux barriers makes the machine increase its maximum torque value. A flux barrier less machine is designed with the down cut kept as it is, as shown in Fig. 7 [19]. The torque value is increased to 14.98 N-m, and ripple is decreased to 0.44 N-m.

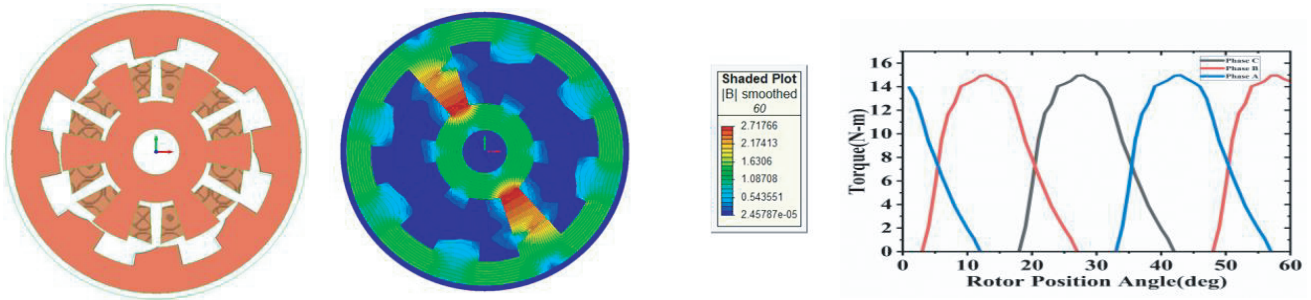

(a) (b) (c)

Figure 7. Asymmetric Rotor Type SRM. (a) FEA model. (b) Flux density and flux pattern of SRM. (c) Torque characteristics of SRM.

4. COMPARISON

The torque ripple of asymmetric rotor is nearly equal to the conventional type rotor, but the maximum and average torque values of asymmetric type rotor are greater than the conventional rotor. Then all the different designed SRMs for propulsion systems are compared. So, an asymmetric rotor SRM is used for the required propulsion system. From Table 1 the asymmetric rotor SRM is better than other types [20].

5. VIBRATION ANALYSIS

The mechanical vibration in the motor caused due to the effect of radial force with the motor is termed as vibration [21]. The natural frequencies of vibration can be by modal method, and it can be determined by,

$$f_r = \frac{1}{2\pi}\sqrt{\frac{K_s}{m_{eq}}}\,\text{Hz} \tag{4}$$

Table 1. Torque characteristics.

Type	$\mathbf{T_{max}}$ (Nm)	$\mathbf{T_{min}}$ (Nm)	$\mathbf{T_{avg}}$ (Nm)	$\mathbf{T_{ripple}}$
Conventional	9.53	6.31	7.92	0.40
FB Embedded No Material	8.65	4.34	6.49	0.66
FB Embedded Non-Magnetic Material	7.72	3.15	5.42	0.84
Increased FB Embedded No Material	10.77	1.97	6.37	1.38
Decreased FB Embedded No Material	13.16	4.49	8.82	0.98
Decreased FB Embedded Non-Magnetic Material	13.55	4.86	9.2	0.94
Asymmetric	14.98	9.51	12.24	0.44

here, m_{eq} is the equivalent mass per area in kg/m^2, and k_s is the spring stiffness coefficient,

$$K_s = \frac{192 * E * I}{l^3} \tag{5}$$

E is the Young's modulus, and I is the moment of inertia, given by

$$I = \frac{b * h^3}{12} \text{ kg} \cdot \text{m}^2 \tag{6}$$

The modal analysis by using Block Lanczos method is executed on electric motor to predict its vibration frequencies. Fig. 8 shows the modal frequencies of SRM.

Table 2 shows the comparison on vibration frequencies of simulation and analytical technique to acquire its efficient. The amplitude of vibration in the proposed machine is estimated by applying radial force to the motor. Fig. 9 shows the boundary condition applied to the motor at shaft as zero displacement and the applied radial forces to the outer tip of the stator poles [22]. Fig. 10 plots the amplitude of vibration and infers that the machine has high amplitude of vibration at mode 1 and mode 2 frequencies.

Table 2. Comparison of FEA and analytical vibration frequencies.

Mode	Frequencies (Hz)	
	FEA	Analytical
1	2117.04	2005.21
2	2723.42	2843.24
3	3340.56	3580.92
4	3958.99	4021.33
5	4379.83	4492.98

6. THERMAL ANALYSIS

The thermal analysis deals with the heat distribution inside the motor. The losses are converted into heat generated value and applied in the coil area as heat generation, so heat is distributed across the motor [23]. The velocity of air in the air gap regions is calculated from the speed of the motor, and it is given by,

$$v = \frac{\pi DN}{60} \text{ m/s} \tag{7}$$

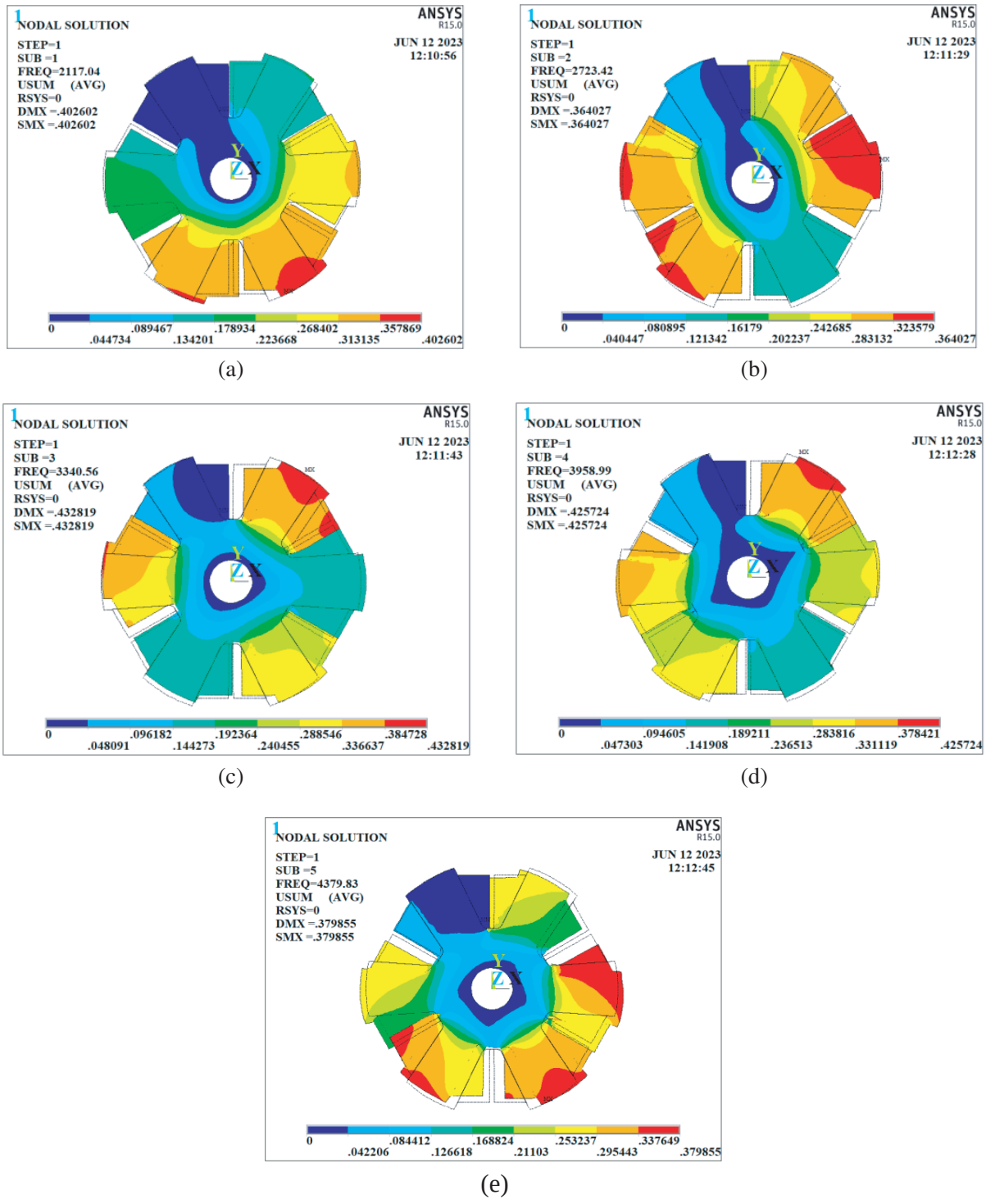

Figure 8. Modal frequencies. (a) Mode 1 at 2117.04 Hz. (b) Mode 2 at 2723.42 Hz. (c) Mode 3 at 3340.56 Hz. (d) Mode 4 at 3958.99 Hz. (e) Mode 5 at 4379.83 Hz.

where D is the air gap diameter of motor, and N is the rotor speed. Table 3 shows the material parameter. Fig. 11 and Fig. 12 show the FEA model for thermal analysis and temperature rise of SRM. In 2D CFD analysis, the component of air velocity at a point $p(x, y)$ in the air gap is given by

$$v_x = v\cos\theta \tag{8}$$

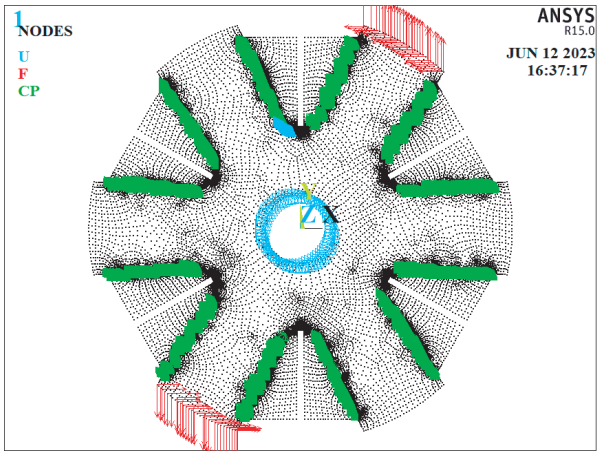

Figure 9. Shows the boundary condition and forces applied to the shaft and stator poles.

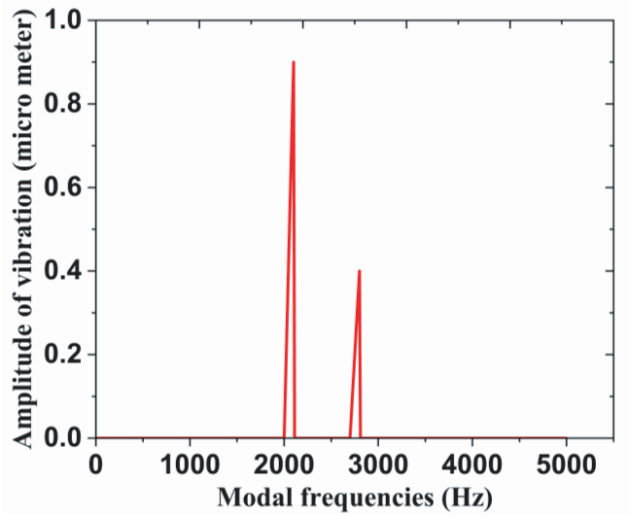

Figure 10. Vibration amplitude.

Table 3. Parameters of materials.

Material	**Thermal conductivity** **(W/m · C)**	**Specific heat** **(J/kg · C)**	**Density** **(kg/m^3)**
M890-50D	25	490	7850
Copper	386	383.1	8954
Shaft	0.025	1005.6	1000
Air	0.026	1005.7	1000

$$v_y = v \sin\theta \tag{9}$$

The heat generation is obtained [24] by,

$$Heat\ \text{generation} = \frac{Losses}{Surface\ Area} \tag{10}$$

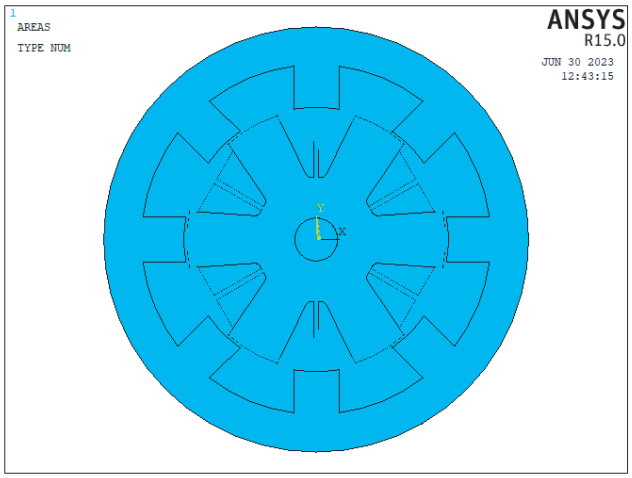

Figure 11. SRM FEA model for thermal analysis.

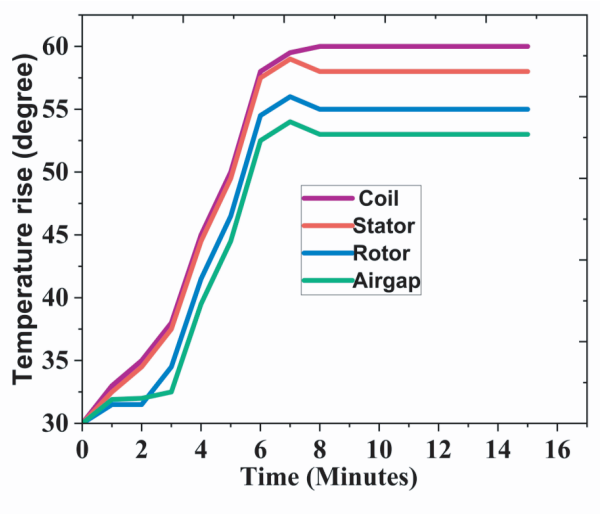

Figure 12. Temperature rise in SRM.

7. EXPERIMENTAL ARRANGEMENT

The experimental arrangement for testing of the proposed motor is implemented in Fig. 13. The driver circuit is shown in Fig. 14. The working of driver circuit is explained in Table 4 [25, 26]. The rated voltage is applied to the motor to run at rated speed of 3000 RPM, and an average current of 0.8 A is fed to the motor which resembles the FEA current profile as shown in Fig. 15.

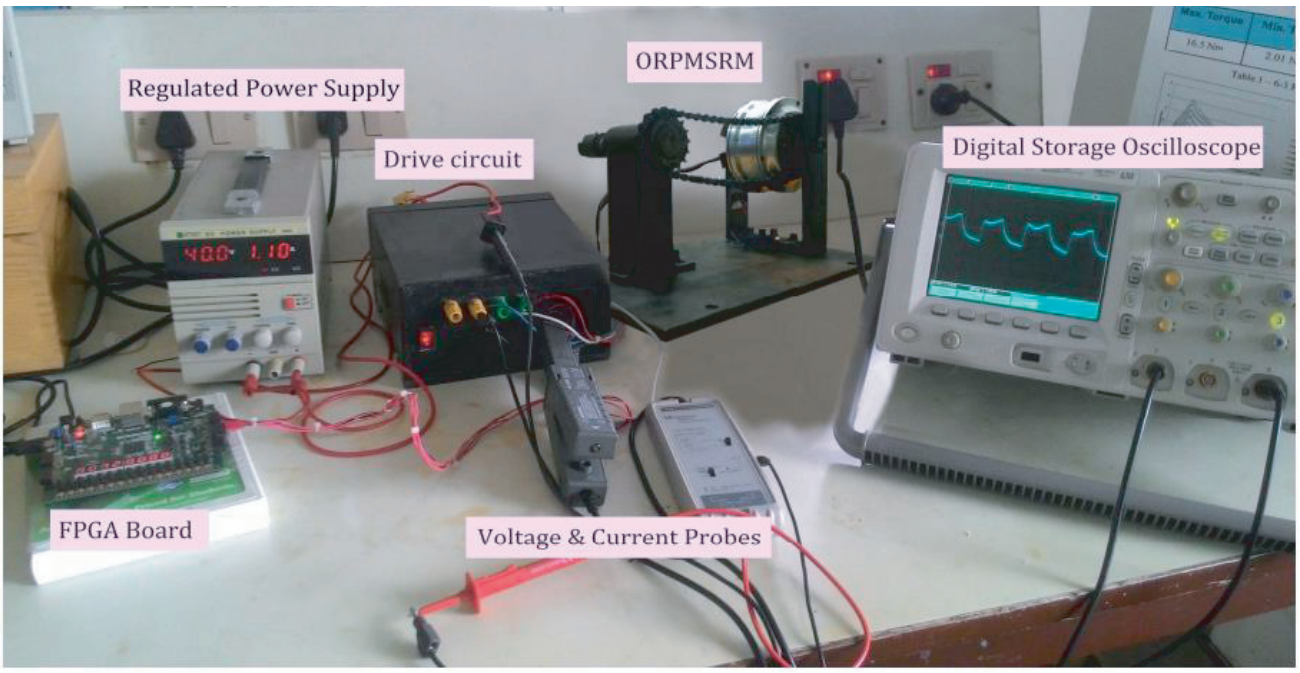

Figure 13. Experimental arrangement.

Table 4. Working of SRM converter.

Degree	Phase A	Phase B	Phase C
0–15	ON	OFF	OFF
0–30	OFF	ON	OFF
30–45	OFF	OFF	ON
45–60	ON	OFF	OFF
60–75	OFF	ON	OFF
75–90	OFF	OFF	ON

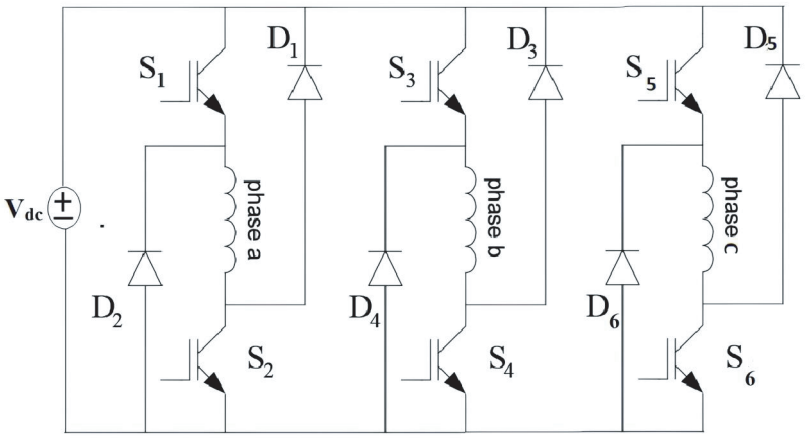

Figure 14. Driver circuit for SRM.

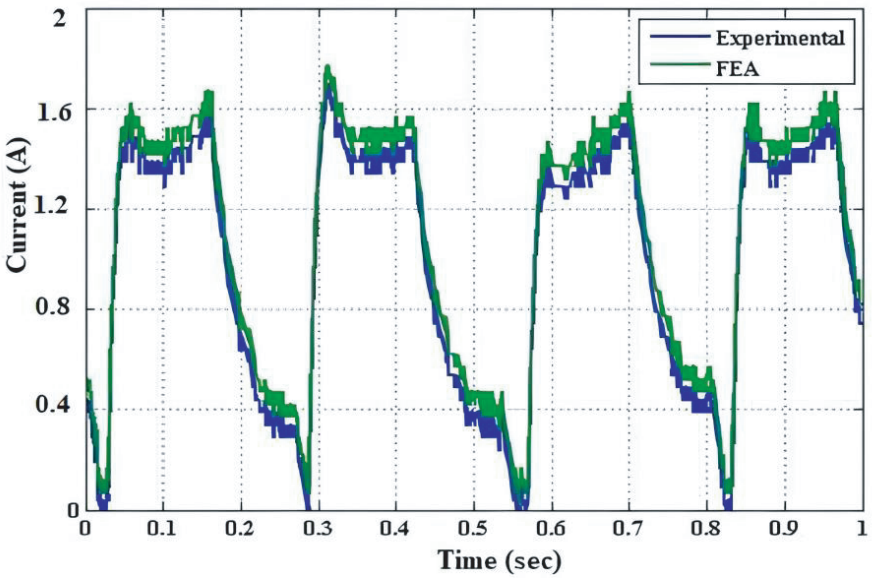

Figure 15. Current profile of FEA and experimental SRM.

8. CONCLUSION

This research article concludes the effect of electromagnetic analysis on switched reluctance outer rotor motor. The geometry optimization technique and the effect of material are incorporated in this study and infer that the asymmetry rotor is superior. Further the vibration analysis is carried out to understand the fact of structural behaviour in the motor, by modal and harmonic analysis for identifying the vibration frequency and its corresponding amplitude. The analysis of losses also considers the effects by investigating the heat flow to a maximum of 60 degrees. An experiment arrangement is implemented to verify the FEA analysis through current characteristics.

REFERENCES

1. Kim, J. H., Y. S. Kwon, S. Lee, et al., "3D hybrid segmented layer modelling of on-load magnetic fields and torques for coreless axial-flux permanent magnet synchronous motor," *IEEE Transactions on Energy Conversion (Early Access)*, 1–12, 2023.
2. Sun, X., Y. Zhu, Y. Cai, Y. Xiong, M. Yao, and C. Yuan, "Current fault tolerance control strategy for 3-phase switched reluctance motor combined with position signal reconstruction," *IEEE Transactions on Energy Conversion (Early Access)*, 1–11, 2023.
3. Ruan, Z., W. Song, L. Zhao, Y. Zhang, and Y. Guo, "A variable switching frequency space vector pulse width modulation control strategy of induction motor drive system with torque ripple prediction," *IEEE Transactions on Energy Conversion*, Vol. 38, No. 2, 993–1003, 2023.
4. Liang, W., P. C.-K. Luk, and W. Fei, "Investigation of magnetic field inter harmonics and sideband vibration in the FSCW IPMSM drive with the SPWM technique," *IEEE Transactions on Power Electronics*, Vol. 33, No. 4, 3315–3324, April 2018.
5. Prabhu, S. and M. Balaji, "Performance analysis of permanent magnet assisted outer rotor switched reluctance motor with non-oriented laminating material for electric transportation systems," *2022 IEEE 2nd International Conference on Sustainable Energy and Future Electric Transportation (SeFeT)*, 1–6, 2022.
6. Arun, V. and S. Prabhu, "Design and vibration analysis on EMS by using Block Lanczos method for humanoid robotics arm applications," *Int. J. Interact. des Manuf.*, 2022.
7. Kurinjimalar, L., M. Balaji, S. Prabhu, and R. Umadevi, "Analysis of electromagnetic and vibration characteristics of a spoke type PMBLDC motor," *J. Electr. Eng. Technol.*, Vol. 16, 2647–2660, 2021.
8. Sivasamy, S., M. M. B. Maria, and P. Sundaramoorthy, "Performance investigation of doubly salient outer rotor switched reluctance motor using finite element analysis," *Circuit World*, Vol. 48 No. 4, 412–424, 2022.
9. Sundaramoorthy, P., M. Balaji, K. Suresh, E. Natesan, and K. Mohan, "Vibration analysis of E-core flux reversal free stator switched reluctance motor," *Circuit World*, Vol. 46, No. 4, 325–334, 2020.
10. Prabhu, S., M. Balaji, and V. Kamaraj, "Analysis of two phase switched reluctance motor with flux reversal free stator," *2015 IEEE 11th International Conference on Power Electronics and Drive Systems*, 320–325, IEEE, June 2015.
11. Sundaramoorthy, P. and M. Balaji, "Analysis and implementation of two-phase flux reversal free doubly salient machine," *Journal of Magnetics*, Vol. 23, No. 3, 350–359, 2018.
12. Sundaramoorthy, P., V. Arun, B. H. Kumar, J. Kavali, and M. Balaji, "Investigations on novel hybrid reluctance motor for electric vehicle applications," *IEEE Canadian Journal of Electrical and Computer Engineering*, Vol. 45, No. 4, 454–465, 2022.
13. Prabhu, S., A. Vijayakumar, A. A. Stonier, G. Peter, S. Dorji, and V. Ganji, "Analysis of isolated phase windings and permanent magnet assists high energy efficient hybrid-reluctance motor for electric vehicle," *IET Electr. Syst. Transp.*, 1–10, 2023.
14. Prabhu, S., V. Arun, M. Balaji, V. Kalaimagal, A. Manikandan, and B. M. Reddy, "Investigations on brushless DC motors for automotive systems," *2023 9th International Conference on Electrical Energy Systems (ICEES)*, 138–142, Chennai, India, 2023.

15. Prabhu, S., V. Arun, M. Balaji, V. Kalaimagal, A. Manikandan, and V. Chandrasekar, "Electromagnetic analysis on interior permanent magnet motor for electrified transportation systems," *2023 9th International Conference on Electrical Energy Systems (ICEES)*, 163–168, Chennai, India, 2023.
16. Prabhu, S., V. Arun, M. Balaji, V. Kalaimagal, A. Manikandan, and V. Chandrasekar, "Performance investigations on synchronous reluctance motor for automotive applications," *2023 International Conference on Power, Instrumentation, Energy and Control (PIECON)*, 1–6, Aligarh, India, 2023.
17. Prabhu, S., V. Arun, M. Balaji, V. Kalaimagal, A. Manikandan, and V. Chandrasekar, "Influence of laminating core materials on internal permanent magnet motor for locomotive systems," *2023 International Conference on Power, Instrumentation, Energy and Control (PIECON)*, 1–4, Aligarh, India, 2023.
18. Prabhu, S., V. Arun, M. Balaji, V. Kalaimagal, A. Manikandan, and V. Chandrasekar, "Electromagnetic analysis on brushless DC hub motor for electrified transportation systems," *2023 9th International Conference on Electrical Energy Systems (ICEES)*, 179–183, Chennai, India, 2023.
19. Prabhu, S., V. Kalaimagal, V. Arun, A. Manikandan, M. Balaji, and V. Chandrasekar, "Impact of laminating core materials on switched reluctance motor for automotive applications," *2023 International Conference on Power, Instrumentation, Energy and Control (PIECON)*, 1–4, Aligarh, India, 2023.
20. Prabhu, S., V. Arun, M. Balaji, V. Kalaimagal, A. Manikandan, and V. Chandrasekar, "Analysis on misc type permanent magnet synchronous reluctance machine for transportation systems," *2023 International Conference on Power, Instrumentation, Energy and Control (PIECON)*, 1–5, Aligarh, India, 2023.
21. Prabhu, S., V. Arun, M. Balaji, V. Kalaimagal, A. Manikandan, and V. Chandrasekar, "Finite element analysis on interior permanent magnet machine for propulsion system," *2023 International Conference on Power, Instrumentation, Energy and Control (PIECON)*, 1–5, Aligarh, India, 2023.
22. Han, J., J. Wang, B. Ge, H. Qi, and X. Bian, "Influence of different control parameters on the flux density and loss of stator core in the switched reluctance motor," *IEEE Access*, Vol. 11, 53624–53633, 2023.
23. Sahu, A. K., A. Emadi, and B. Bilgin, "Noise and vibration in switched reluctance motors: A review on structural materials, vibration dampers, acoustic impedance, and noise masking methods," *IEEE Access*, Vol. 11, 27702–27718, 2023.
24. Kumar, P., M. Israyelu, and S. Sashidhar, "A simple four-phase switched reluctance motor drive for ceiling fan applications," *IEEE Access*, Vol. 11, 7021–7030, 2023.
25. Lenin, N. C., "48-Volt energy efficient domestic appliances with flux switching motor drive system — Design, simulation, and comparison," *IEEE Access*, Vol. 10, 81568–81580, 2022.
26. Ramesh, P. and N. C. Lenin, "High power density electrical machines for electric vehicles — Comprehensive review based on material technology," *IEEE Transactions on Magnetics*, Vol. 55, No. 11, 1–21, Art No. 0900121, November 2019.